공학석사학위논문

# 중 저온에서의 지르코니아를 기반으로한 양성자 전도성 전해질 특성 분석

# Electrochemical Optimization of Zirconium based Protonic Conducting Electrolyte for intermediate Temperature Fuel Cell

2019년 2월

서울대학교 대학원

기계항공공학부

소 지 현

# Abstract

# Electrochemical Optimization of Zirconium based Protonic Conducting Electrolyte for intermediate Temperature Fuel Cell

Ji Hyun So
Department of Mechanical and Aerospace Engineering
Seoul National University

There are two types of electrolyte; protonic conductor electrolyte and ion conductor electrolyte. The BaZr0.8Y0.2O3− (BZY) powder, a protonic conductor candidate electrolyte for intermediate temperature (500–700 °C) solid oxide fuel cells (IT-SOFCs), was mixed with (Y2O3)8 (ZrO2)92 (YSZ) powder, oxygen ion conductor candidate, by ball milling technique then be a BZY-YSZ mixed pellet by different weight ratio. The ratio of BZY to YSZ was 25:75, 50:50,and 75:25 and 100:0 and 0:100 were made for reference of raw data. The powders were sintered escalated

temperature at 600,1000, for 5 hours and 1400 °C for 10 hours. The sintered pellets were shrunk. The phase composition of the resulting specimens was investigated using X-ray diffraction (XRD) analysis. Microstructural characterization was performed using field emission scanning electron microscopy (FE-SEM). To analyze the grain, Energy dispersive X-ray spectroscopy (EDS) was used to distinguish the grains. Fuel cell polarization curves on symmetric Ag/BZY-YSZ/Ag cells of different weight ratio pellets were measured at 500–650 °C.

**Key Words** : Solid Oxide Fuel Cell, Fuel Cell, Protonic Conducting Electrolyte, PCE, PCFC

**Student Number:** 2017-20242

# Table of Contents

# List of Tables

# List of Figures

# Chapter 1. Introduction

## 1.1. Study Background

The need for a new energy source was always claimed to have better energy density since the primary energy source is limited. From the 1st Industrial Revolution up to now, the energy source had been changed from woods to coal to oil that produced electricity. However, as much as attention towards the new energy source, but also side effects of usage of non-renewable energy, fossil fuels, were on target to avoid. The serious environmental problems from the usage of non-renewable energy are following; global warming, air pollution, and desertification. With a limited amount of petroleum and its caused problem, the renewable and eco-friendly energy source was required for better sustainability of human beings. Excluding nature replenished energy source, solar, wind, tides, rain, and others, hydrogen is spotted as a next-generation energy source in the various field. Among the several candidates, hydrogen and its energy have a high potential of becoming the primary energy source in next generation, since the hydrogen is one of the most common elements in the Earth and can be obtained from various resources. To generate electricity from the hydrogen energy, the fuel cell is now known as the replacement of

petroleum fuel or any power source for the electricity. Fuel cells have been explored as new power source or energy conversion devices in utilizing hydrogen fuel.

Within different kinds of fuel cell, basic of fuel cell is that this device is generated electricity by a chemical reaction that take place through anode, electrolyte and cathode. A single fuel cell has two electrodes at sides of the cell, anode and cathode, and electrolyte in between the electrode. When the fuel, hydrogen atom, reached at the anode side, one hydrogen atom breaks into two hydrogen ions and two electrons. These electrons from anode, travel to the external circuit to provide electricity. In the cathode side, on the other hand, one oxygen molecule gets four electrons and becomes two oxygen ions. Then, these oxygen ions pass through the electrolyte and meet hydrogen ions at the anode/electrolyte interface to produce water as exhaust.

Anode: $2H_2 + 2O_2^-(from\ cathode) \rightarrow 2H_2O + 4e^-$

Cathode: $O_2 + 4e^- \rightarrow 2O_2^-$

Overall: $2\ H_2 + O_2 \rightarrow 2\ H_2O$

Depending on the electrolyte materials, hydrogen ions can also travel to the cathode/ electrolyte interface. In this case, water is produced on the cathode side. Since there is no other product besides water in the whole process, we can get electricity ecofriendly.

### 1.1.2 Solid Oxide Fuel Cell

Traditionally, there are five different types of fuel cell; PEMFC, PAFC, AFC, MCFC, SOFC (PEMFC: polymer electrolyte membrane fuel cell, PAFC: phosphoric acid fuel cell, AFC: alkaline fuel cell, MCFC: molten carbonate fuel cell, SOFC: solid oxide fuel cell). Each fuel cell has its own characteristic relating the component materials and its operating temperature. Depends on electrolyte and operating temperature, the types of fuel cell is divided, as it shown in Table 1.

| | PEMFC | PAFC | AFC | MCFC | SOFC |
|---|---|---|---|---|---|
| **Electrolyte** | Polymer membrane | Lipid $H_3PO_4$ | Lipid KOH | Molten carbonate | Ceramic |
| **Charge Carrier** | $H^+$ | $H^+$ | $OH^-$ | $CO_3^{2-}$ | $O^{2-}$ |
| **Operating Temperature** | 80℃ | 200℃ | 60-220℃ | 650℃ | 600-1000℃ |
| **Fuel Compatibility** | $H_2$, methanol | $H_2$ | $H_2$ | $H_2$, $CH_4$ | $H_2$, $CH_4$, CO |

Table 1. Major Fuel Cell Types [1]

Comparing other major fuel cells, SOFC has advantages with highly

efficient energy system and fuel flexibility. However, the operating temperature of the SOFC is relatively high (600℃~1000℃), which limits the commercialization due to the thermal stability, the long start-up time, and the sealing problems.

To lowering the operating temperature of the SOFC, many researches have been focused on fabricating thin film electrolytes as well as fabricating a film having a good ionic conductivity. By fabricating the thin film to be electrolyte up to tens of nanometers to several micrometers, the ion conductivity of the electrolyte is improved as well as its electrochemical performance. Besides lowering the thickness, selection of material is key to improve the conductivity. For SOFC, 8 mol% yttria-stabilized zirconia (YSZ) is notably used as electrolyte with its number of compelling advantages; high chemical stability, high ionic conductivity, stability compatibly in oxidizing and reducing environment, and high compatibility with the electrode material [2-4]. There is no doubt that YSZ being easily approachable material for electrolyte. In aspects of material, its mixed ratio or different combination of materials have been investigated for long to find better conductivity. Other than material selection, the research trends are shifted towards proton conducting electrolyte. Figure 1 shows that SOFC electrolyte can be approached in two ways. One is focused on oxide- ion conducting electrolyte, and other is working with proton conducting

electrolyte.

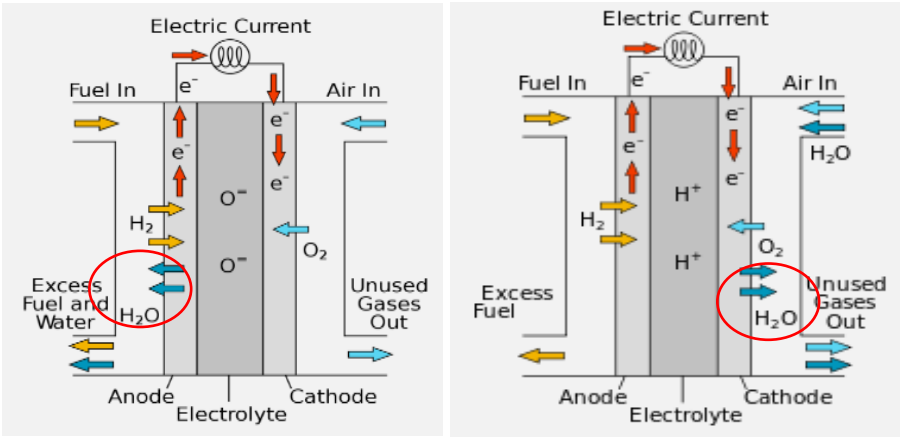


Figure 1. Schematic of SOFC and PCEs application[29]

# Chapter 2. Experiment Details

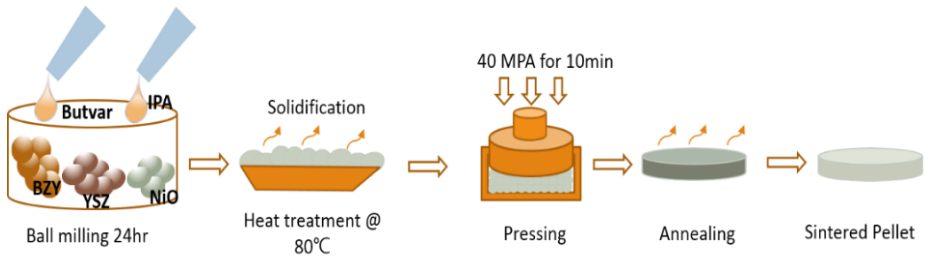


Figure 2. Short schematic of fabrication of BZY-YSZ hybrid pellet

Figure 2 briefly shows the procedure of fabrication of BZY-YSZ powder with coagulant solutions and hybrid pellet to be tested for electrochemical performance. In this section, each step is elaborated with powder details and experimental obtained details.

## 2.1. Preparation of BZY-YSZ powders

For BZY-YSZ composite pellet, commercial NiO (Wako, USA), butvar (Sigma Aldrich, USA) $BaZr_{0.8}Y_{0.2}O_{3-\delta}$ (Kceracell, South Korea) and $(Y_2O_3)_8$ $(ZrO_2)_{92}$ (YSZ) (Kceracell, South Korea) composite powders were mixed with different weight ratios regarding Table 2. From now on,

$BaZr_{0.8}Y_{0.2}O_{3-\delta}$ (BZY)- $(Y_2O_3)_8$ $(ZrO_2)_{92}$ (YSZ) is named as BZY-YSZ and acronym is followed by a number indicating the weight percentage of BZY in the composite powder. The hybrid pellet is named under following weight ratio of BZY to YSZ; 25BZY (25:75), 50BZY (50:50), 75BZY (75:25), raw BZY* (100:0), raw YSZ* (0:100), respectively. The solvent, Isopropyl alcohol, was adding to each of BZY, 8 mol% Yttria Stabilized Zirconia and other mixed chemical composition with different weight ratio till the mixture would be slurry.

| | Powder wt% | | | |
|---|---|---|---|---|
| | YSZ | BZY | NiO | Butvar |
| 25BZY | 75 | 25 | 1 | 0.5 |
| 50BZY | 50 | 50 | 1 | 0.5 |
| 75BZY | 25 | 75 | 1 | 0.5 |
| BZY* | 0 | 100 | 1 | 0.5 |
| YSZ* | 100 | 0 | 0 | 0.5 |

Table 2. BZY-YSZ pellet composition weight ratio

This mixture was mixed for 24 hours via ball milling (GLBM-G, Global Lab, South Korea) to obtain proper homogeneity. The miller was

operated at 200 rpm with 15 grams of (94.8% $ZrO_2$) zirconia ball of 2mm diameter (Samhwa ceramic, South Korea) and 10g of mixed powder excluding isopropyl alcohol weight in each milling jar. Before being transferred into oven plate, zirconia ball was split from diluted chemical composition through 1mm stainless steel mesh. The solution without the zirconia balls poured into foil covered plate for solidification was located in the oven, drying at 80℃ to remove the isopropyl alcohol. For 6 hours of solidification, the greenish solid mixture was hand ground by ceramic bowl and crusher to obtain fine powder particles. However, additional hand grind prior to making a new pellet is necessary.

## 2.2 Fabrication of hybrid pellet

For the preparation of a pellet, around 0.3g of mixed powder from prior step was re-grinded as one step. To optimized the thickness of pellet, three different weight powder,0.7g, 0.9g, 1.1g, were pressed to be a pellet and tested. Later, 0.9g of mixture powder was selected throughout the experiment. Combining 0.9g ,three ground steps, BZY-YSZ powder was first pressed under 40MPa into a substrate in a steel die with 15mm diameter for 10 minutes. With 0.9g of BZY-YSZ, optimized thickness of pellet was

1.4 mm in this stage. After that, the pellet was sintered at 600℃, 1000℃, and 1400℃ with increase of 2.5°C $min^{-1}$ stepwise. At first two steps, each step was on hold for 5 hours, but at 1000℃, the step was remained for 10 hours for sintering. After 29.3 hours of sintering, the furnace temperate was gradually decreased to 0℃ in 9.2 hours. Within sintering process, obtained BZY-YSZ pellet shrink to a diameter of 13mm and thickness of 1.3mm in Figure 3.

Figure 3. Comparison pellet picture of before/after sintering

## 2.3 Fabrication of Symmetric Cell

The sintered pellet was fabricated into symmetric cell with anode/electrolyte/cathode assemblies by spreading Ag paste on both sides of pellet. A 4mm width brush (Hwahong, South Korea) was dipped into Ag

paste (Aremco Products, USA) for 5 even coat. The amount of Ag paste per coat was consistent, thus both sides of the symmetric cell was even. Then bent silver wire to be spiral shape was flattened by hammer to maximize the conductivity was attached both side of pellet on top of Ag paste. The 5kg metal was placed on top of these assemblies; the silver wires and the pellet were stuck well with Ag paste.

## 2.4 Symmetric Cell Characterization

The fabricated symmetric cells were tested in our custom-made probe station starting at 500 ℃ to 650℃ by 50℃ increase. There were two types of the test, one was under supplying hydrogen and another was under air condition. In first case, the symmetric cells were firstly heated up to 500 ℃ in 45 minutes and kept at 500 ℃ for 10 minutes while hydrogen was supplying to the anode chamber with a flow rate of 50 sccm, but the cathode was exposed to the ambient air. Another types of tests were under ambient air environment. Each test was consisted of 25BZY, 50BZY, 75BZY, raw BZY*, and raw YSZ*. Detailed figure of the probe station is shown in Figure 4.

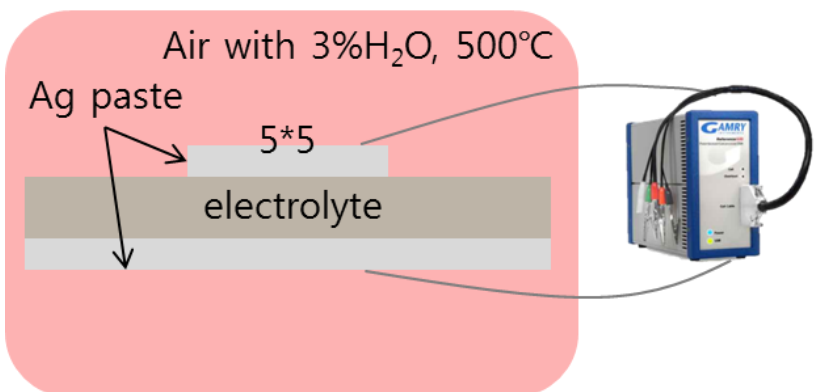


Figure 4. Schematic of Pellet and probe station

Electrochemical impedance spectroscopy (EIS) data of the cells was plotted with a Gamry system, multichannel potentiostat **(VMP3 Bio-Logic Co.)** in the frequency range between from 0.02 Hz to 1 MHz, with an AC voltage amplitude of 30 mV. The impedance spectra were fitted with Gamry Echem Analyst software. For analysis towards microstructure and phase analysis, following analysis were used. X-ray fluorescence (**XRF, XRF-1800)**, X-ray diffraction **(XRD, X'pert Pro**) analysis were used to identify the phase structures of the as-prepared powder and pellet. The phase composition of these powders after electrochemical test was analyzed by XRD. Scanning electron **microscopy (SEM, Hitachi S-4800)** was used to observe the morphologies of BZY-YSZ grain boundary of the symmetric cell after the test. Energy dispersive X-ray spectroscopy **(EDS) analysis** was used to examine the possible element diffusion at BZY-YSZ interface.

# Chapter 3. Discussion and Analysis

## 3.1 Crystalline Analysis

From previous Figure 3, the pellet is shrunk as the chemical reaction is occurring during sintering process. As the temperature goes up to 1400 ℃, the BZY and YSZ powders could result the new material which is checked with EDS as shown in Figure 5. In Figure 5, BZY 25 is analyzed for crystalline analysis. BZY peaks are represented with red triangle while YSZ peaks are green rectangle. Both BZY and YSZ are occurring at (110) very closely. Other than that, there are no typical peaks to represent other material except BZY and YSZ which concludes that there are no other chemical reactions at any grain boundaries or interconnections. Along the crystalline analysis, microstructure of shrunk pellet is analyzed. NiO does not occur as peak in EDS due to its small weight percent. The purpose of adding NiO is its characteristic of sintering aid. When it post sinter-reactive with $BaZr_{0.8}Y_{0.2}O_{3-\delta}$ (BZY), BZY-NiO composite enhance to increase densification of deposited BaZrO3 films in this case its grain boundary that leads to have better electrochemical performance, especially proton conducting fuel cell [5-6].

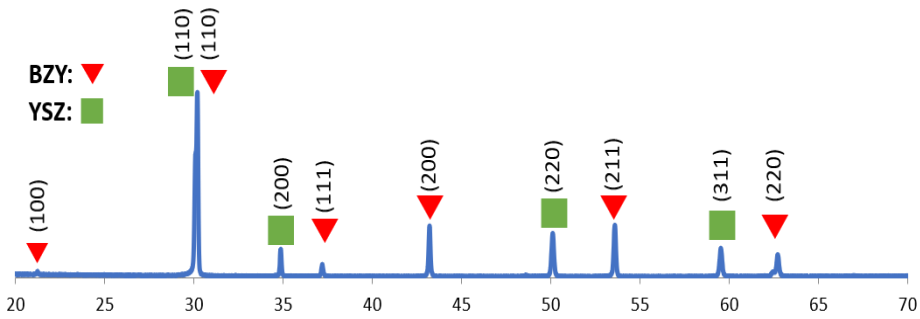


Figure 5. XRD data of BZY 25

## 3.2 Microstructure

From Figure 6-10, SEM image shows the microstructure of YSZ raw, BZY raw and 3 different BZY -YSZ ratio pellet in order of BZY 25-YSZ 75, BZY 50-YSZ 50, and BZY 75-YSZ25. Figure 6 is SEM image of raw YSZ and Figure 7 is SEM image of raw BZY. Comparing two Figures, grain size from Figure 7 is far larger than its from Figure 6. Also, Figure 7 is porous than another. From the those two figures, mixed BZY-YSZ SEM images are expected to be more denser than Figure 6 and 7 due to NiO sintering process. Figures 8-10, microstructure contains two types of grain, larger as background and smaller one on top of background or in between larger grain boundaries. Figure 8, BZY 25, became much denser than previous Figure 7, BZY raw images, with the larger grains from Figure 8 is actually smaller than grains form Figure 7. Also, like the expectations, there are another

grains on top of each other to block the porous space. In Figure 9, microstructure of BZY 50 shows much smaller grain size compare to BZY 25. Also, as the weight ratio of BZY is increased, BZY 50 seems to be denser and tended to have intergranular fracture mode that is strength of grain boundary region is less that its internal grain [8].

Unfortunately, there is no direct or proportional relationship between the amount of BZY and density or grain size from microstructure. Within these SEM images, grain size from BZY 25 and BZY 75 from Figure 11 seems larger than grains from BZY 50. Microstructure of BZY 50 shows denser than but similar grain shape and size to YSZ Raw from Figure 6. Increment of YSZ powder, little grains on top of base grains from YSZ is happened to be on BZY 50 base grains. Whether smaller grain is BZY or YSZ, Figure 9 is well per-collated among others which can be translated as BZY and YSZ is well connected to improve the performance of hybrid electrolyte. In Figure 10, the larger grains are bigger than larger grains from Figure 9, but in between boundary grains or tentatively smaller grains on top of base grains are smaller than BZY 25 from Figure 8.

The conductivities of crystalline materials are affected by its grain and boundary. Since this experiment was run with pellet, it is illustrated for bulk and grain boundary phase. The grain boundary of BZY and YSZ did not show any micro cracks, according to previous Figure 6-10. Another factor that can affect grain boundary is second phase impurities, and it is

checked by EDS analysis also for other reasons [9-11].

To analyze grain components whether larger base area is BZY or not, EDS analysis was done along with FE-SEM. Figure 11 represent the element analysis graphs and related SEM images. In Figure 11 (a), larger grains from BZY 25 was composed of Ba, Y, Zr, and O elements which were main elements for $BaZr_{0.8}Y_{0.2}O_{3-\delta}$ (BZY). While the smaller grains that on top of the BZY grains, was resulted without Ba peak, which was concluded to be $(Y_2O_3)_8$ $(ZrO_2)_{92}$ (YSZ) grain. The presence of Ag peak was found in Figure 11 (b). This sample was post electrochemical test, the pellet surface was lightly covered with Ag paste, then sand down for EDS analysis. However, remained Ag was discovered in the peak along other Y, Zr, and O. According to EDS analysis, larger grains from Figure 8 were concluded to be BZY grains and smaller grains were YSZ. The content of NiO was so low, and it was diffused after sintering process. Likewise, BZY 25 sample, other two hybrid sample result that larger grain part shows Ba peaks and smaller peaks excluded Ba peaks. For Figure 11, the impurities on grain boundaries was not occurring which can enhance the ionic conductivity of the electrolyte. In dense yttria-doped zirconia electrolyte, there was a trend reported that increment of conductivity at interface with decrement of crystallite size till nanometer size [12-13]. Even though, this experiment does not define the relationship between the concentration of BZY and its grain size or density, the general studies about grain size effect which tells

that the better ionic conductivity with the reduced grain size introduce that BZY 25, BZY 50 and BZY 75 might have better conductivity than its raw samples [14-17]. Previous studies about nanocrystalline zirconia-based materials states that electrical conductivity is increased with decreased of grain size instead of ionic conductivity [18].

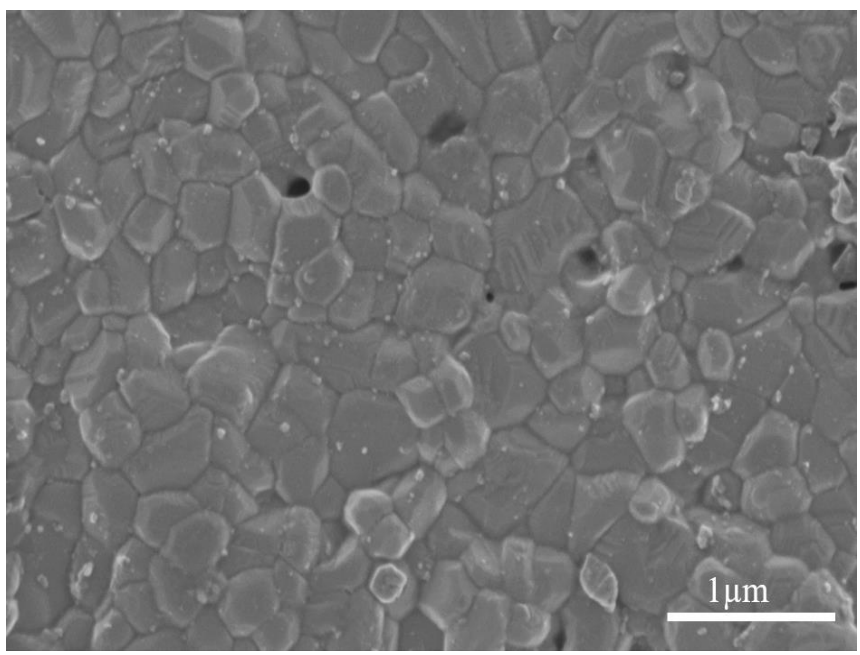


Figure 6. SEM image of YSZ

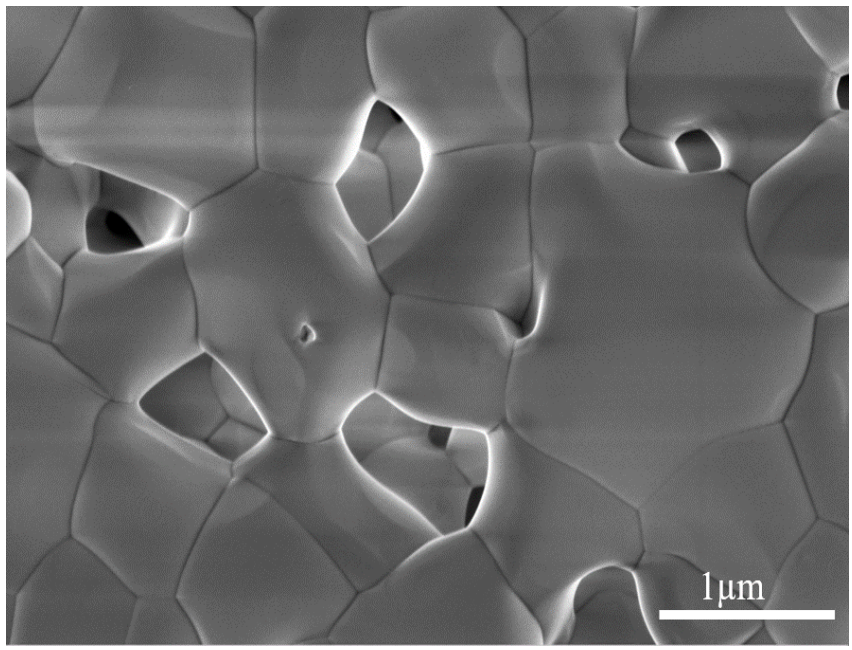


Figure 7. SEM image of BZY

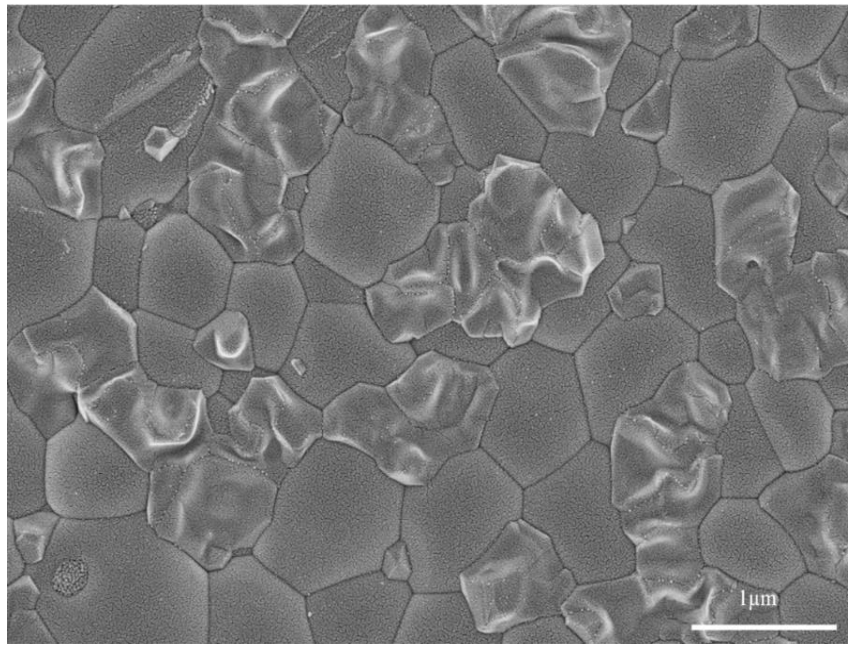


Figure 8. SEM image of BZY 25

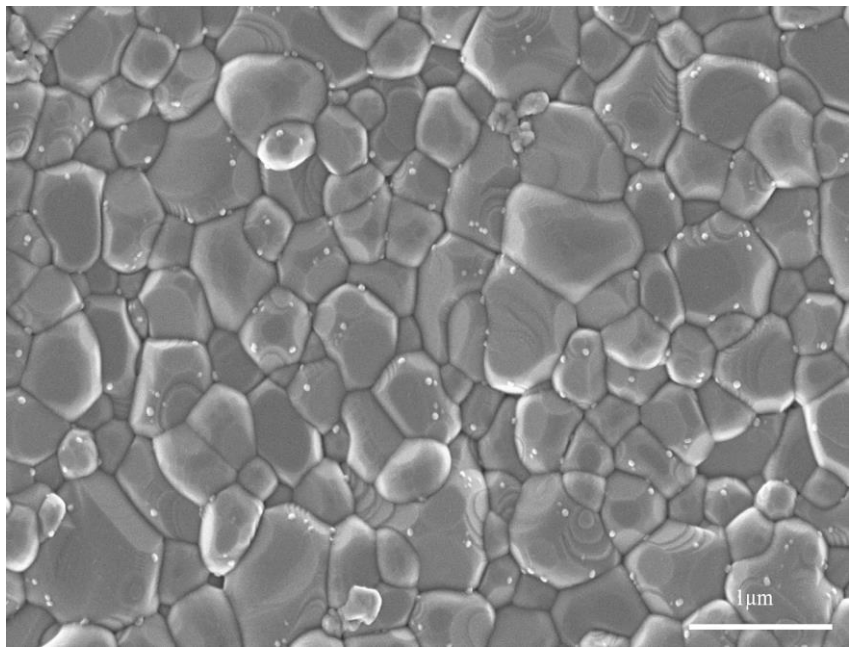


Figure 9. SEM image of BZY 50

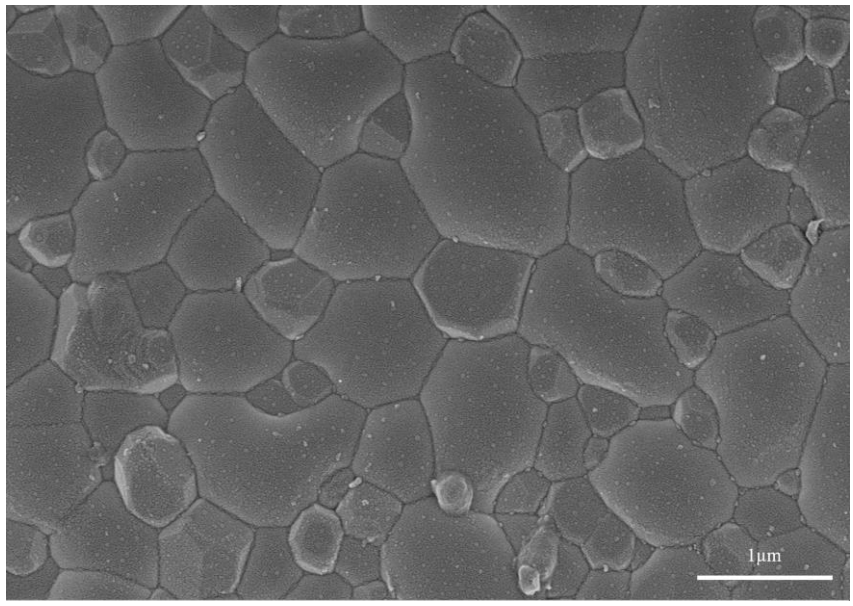


Figure 10. SEM image of BZY 75

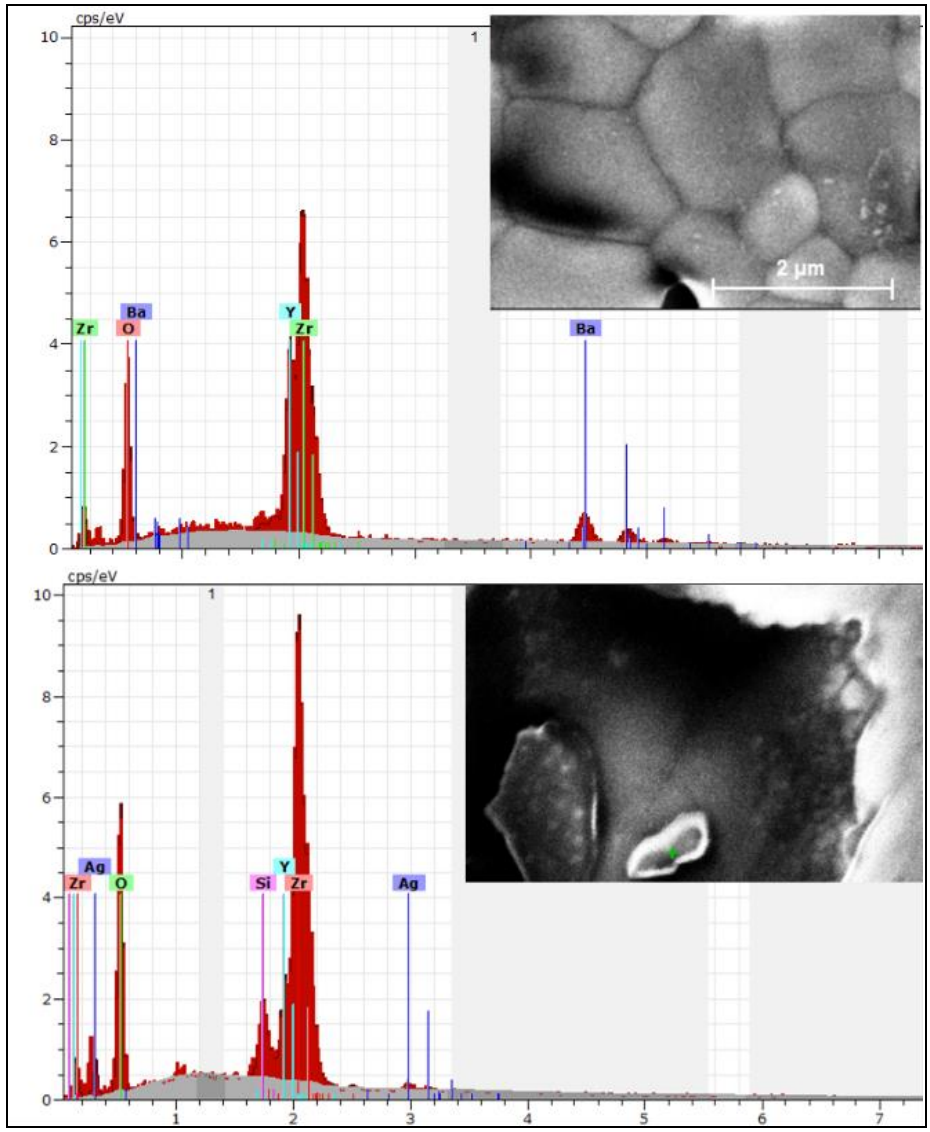


Figure 11. EDS graphs and related location image. a) Top image with larger boundary b) Below image with small grain

## 3.3 Electrochemical Analysis

### 3.3.1 Electrochemical Analysis on Air condition

According to previous studies about grain boundary, grain size and its relation to electrical performance, hybrid samples that are denser and smaller grain size than those of raw YSZ, and BZY resulted better conductivity.

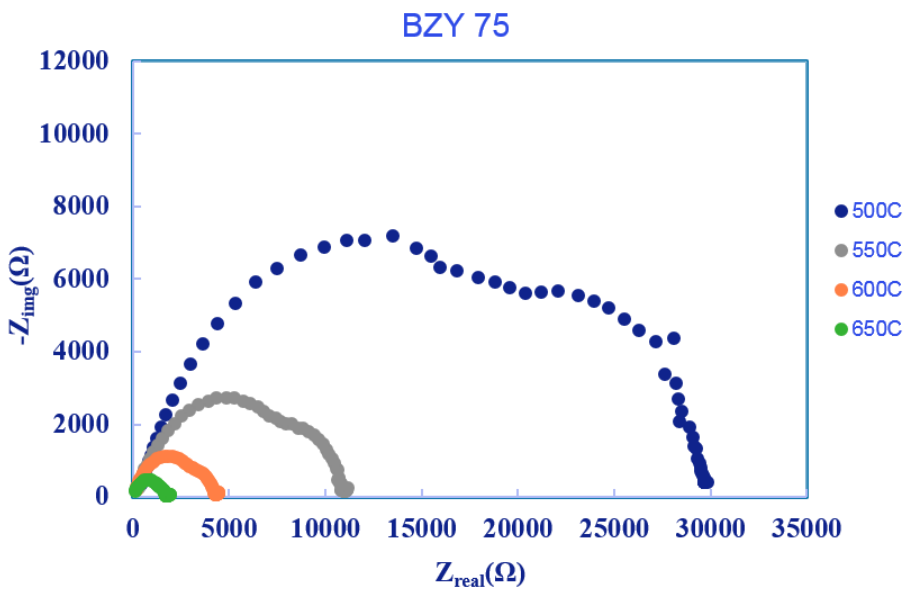


Figure 12. EIS graph of BZY 75 in 500℃ -650 ℃, Air condition

Impedance spectra in a Nyquist plot is shown in Fig. 12 for the BZY 75 sample at 500℃ -650 ℃ under air condition of both anode and

cathode. At 650℃, the spectrum consists of grain boundary polarization, bulk conductivity, and conductivity of electrode in this case the painted Ag layer on top of each pellet side. Since BZY is well known for good protonic conduction, it seems to be strongly hindered in the grain boundary of the BZY-YSZ electrolyte. From Figure 13 -16 shows the Nyquist plot for each temperature range.

Throughout the temperature in Figure 13-16, the bulk and grain boundary contribution arcs were merged into one rough semicircle and finally led to a high frequency resistance. The intercept with the real axis (x-axis) was measured as the ohmic resistance of the cell, which includes the electrolyte resistances. The low frequency intercept corresponds to the total resistance of the cell. Since this experiment is symmetric cell with spreading Ag paste for electrode, polarization resistance was not in scope. The polarization resistance is calculated from the difference between the high frequency and low frequency intercepts with the real axis [19-23]. As shown in Figure 12, polarization resistance was decreased with increasing the temperature.

In Figure 13, at lowest temperature among other condition, BZY 75 shows the largest polarization resistance. To observe the raw materials and other hybrid material, Figure 14-16 did not include BZY 75 which already fully shown in Figure 12. As shown in Fig. 14-16, the BZY 25 electrolyte showed the best electrochemical performance against YSZ in the whole

testing temperature range, indicating that the best weight ratio for BZY and YSZ is 25:75.

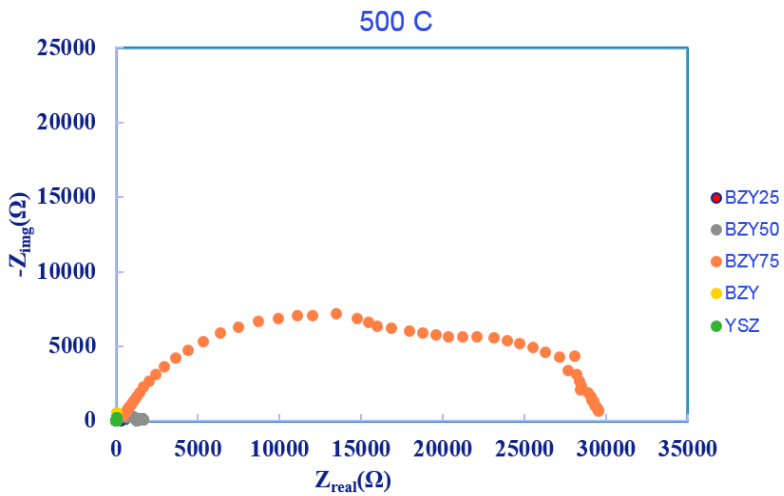


Figure 13. EIS graph of 500℃ Air condition

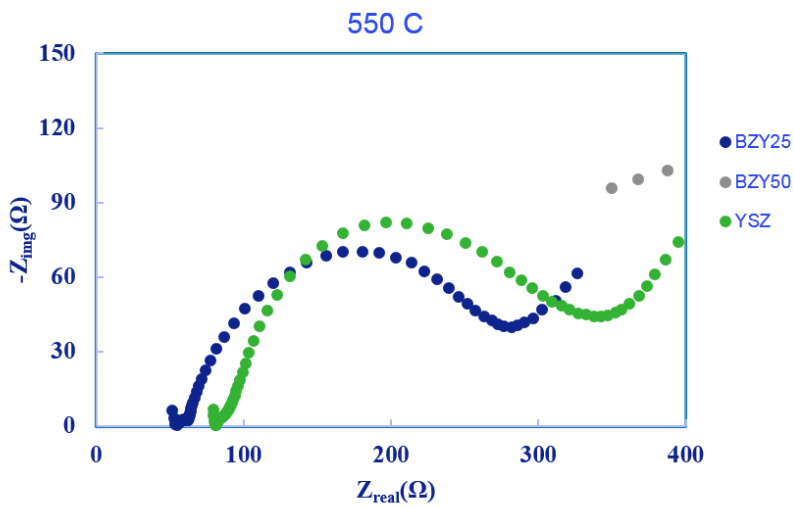


Figure 14. EIS graph of 550℃ Air condition

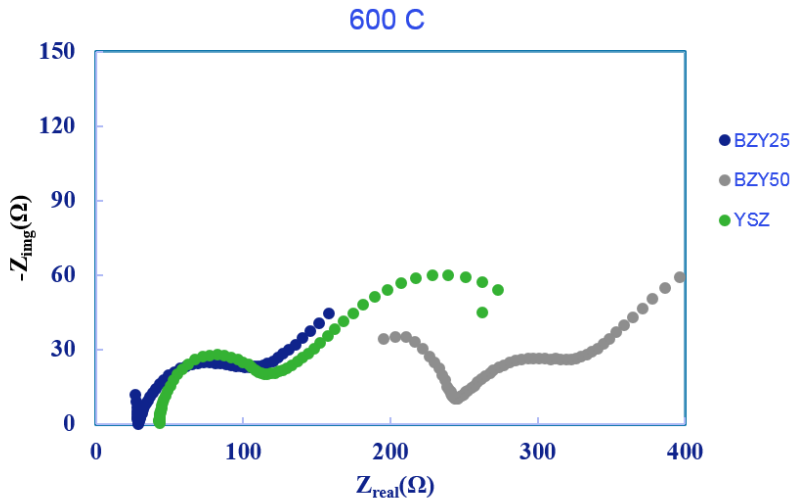


Figure 15. EIS graph of 600℃ Air condition

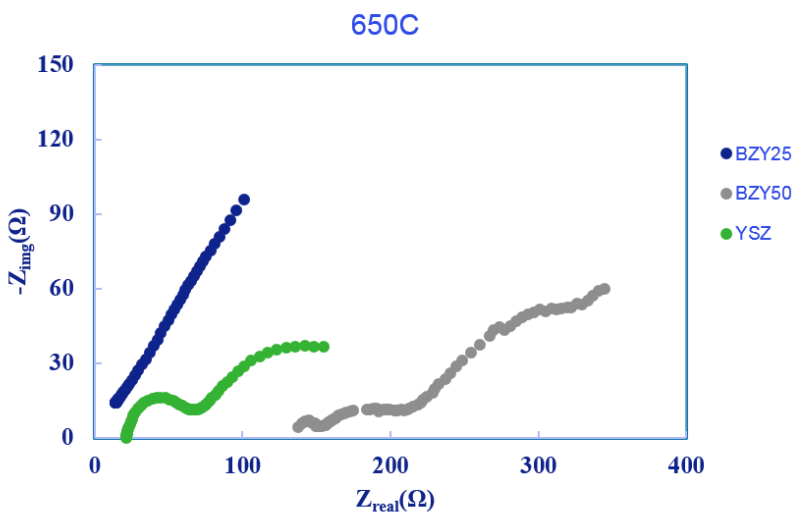


Figure 16. EIS graph of 650℃ Air condition

### 3.3.2 Electrochemical Analysis on $H_2$ condition

In Figure 17-21 are the Impedance Nyquist plot that run under common solid oxide fuel cell environment at 500℃ -650 ℃ in wet (5%) $H_2$. To check the resistance relating to grain boundary and bulk, Figure 17 merge all the data for BZY 75 into one plot. As above Air condition, the total resistance is decreasing as the temperature is increasing. From Figure 18 -21 shows the Nyquist plot for each temperature range.

The studies states that BZY conductivity is dominated by proton conduction under a wet hydrogen atmosphere [24-25]. Therefore, $H_2$ condition is favorable to high BZY concentration hybrid pellet.

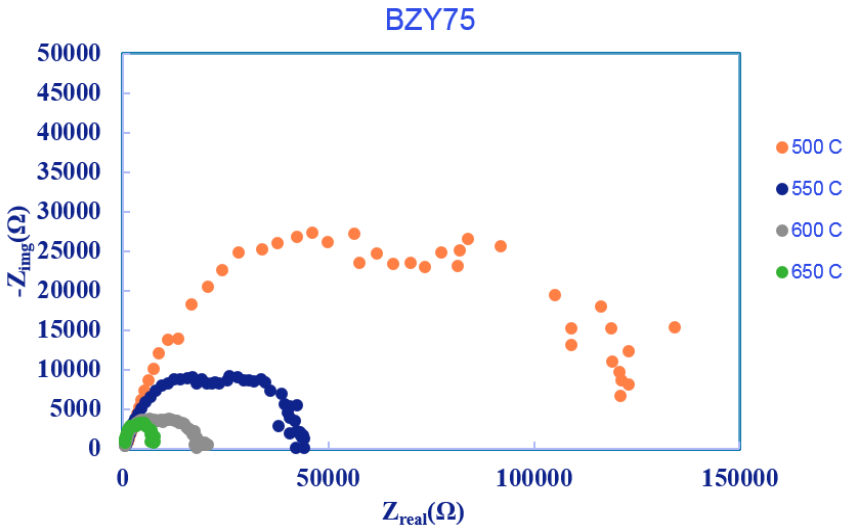


Figure 17. EIS graph of BZY 75 in 500℃ -650 ℃, $H_2$ condition

However, based on Nyquist plot from Figure 18-21 did not show any conductivity difference between BZY 25-75. The intercept with real axis of BZY 25 was far behind the raw YSZ. Therefore, the hybrid BZY samples were not influenced by its favorable environment, $H_2$ condition. Among the hybrid BZY-YSZ pellets, indicating that the best concentration ratio for BZY and YSZ is again 25:75.

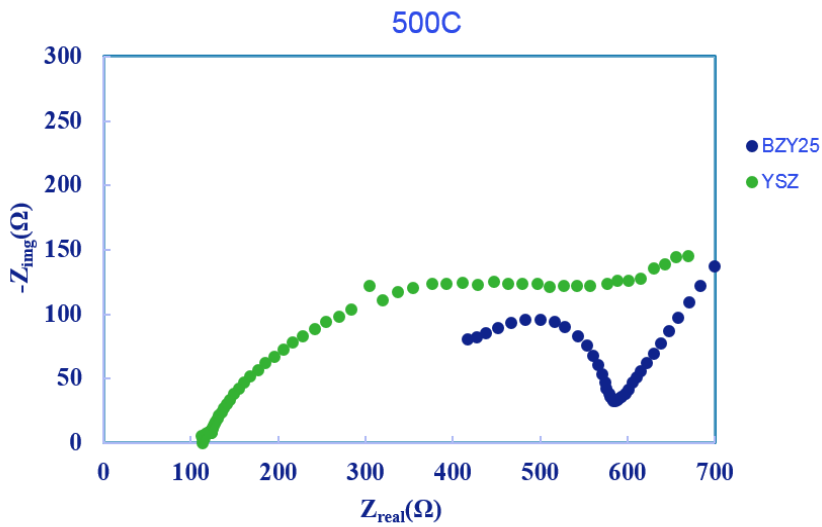


Figure 18. EIS graph of 500℃ $H_2$ condition

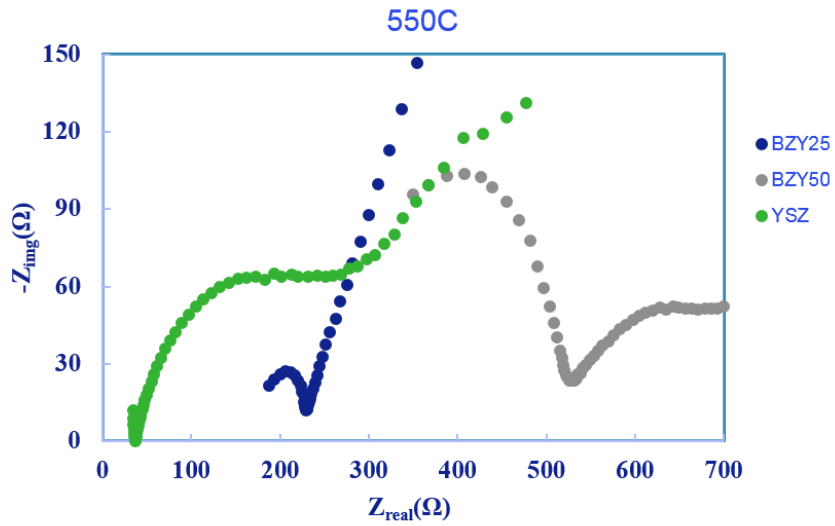


Figure 19. EIS graph of 550℃ $H_2$ condition

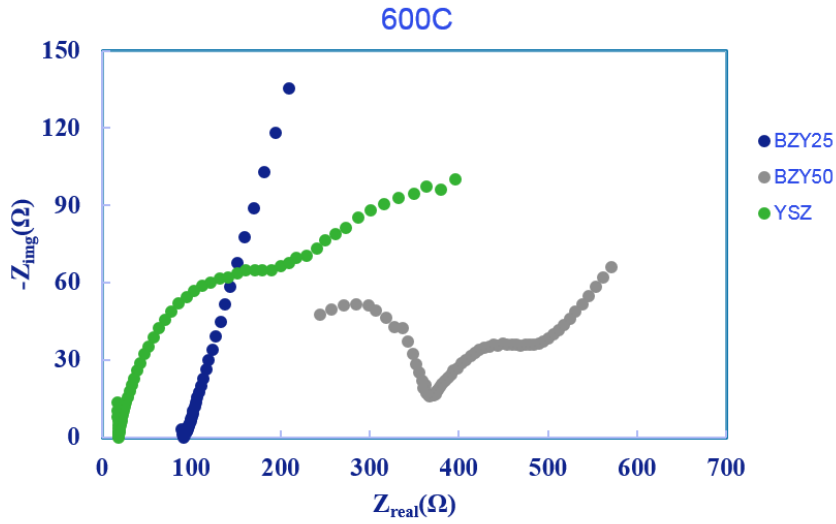


Figure 20. EIS graph of 600℃ $H_2$ condition

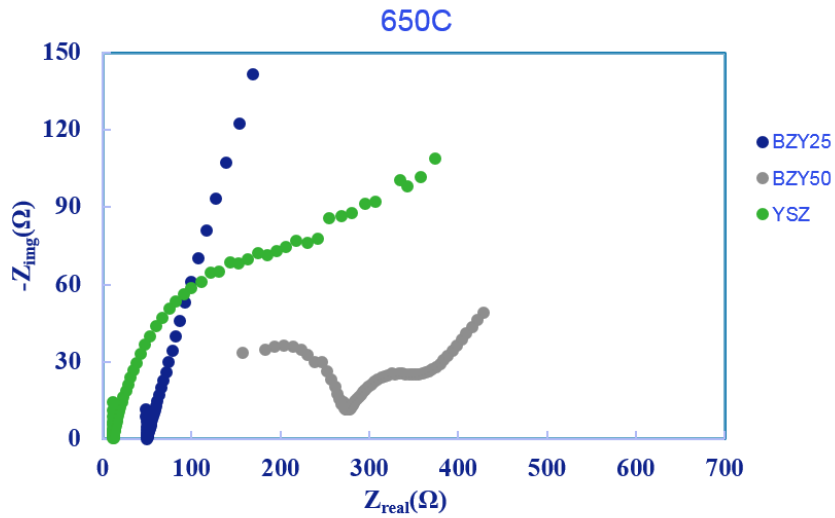


Figure 21. EIS graph of 650℃ $H_2$ condition

## 3.4 Ionic Conductivity

### 3.4.1 Ionic Conductivity Analysis on Air condition

After evaluating the resultant Nyquist plots under ambient air and wet hydrogen condition, the total ionic conductivity of tested samples was calculated to have Arrhenius plot. Arrhenius plot is consisted of calculated ionic conductivity by equation 1 as a function of inverse temperature [26 ] .

$$\sigma_{total} = \text{Pellet thickness} / (\text{Surface Area} \cdot R_{elec}) \quad (1)$$

In Figure 22, the ionic conductivity on ambient air condition was highlighted that BZY25 with green dots were on top of BZY raw with brown dots in most temperature range except 500℃, but it still has higher

conductivity than raw YSZ at 500 ℃. Typically, the well per-collated nanocomposite electrolyte shows that 5 times of ionic conductivity performance comparing to its raw electrolyte [27-28]. However, this case was used by symmetric cell that is hard to result such an improvement but a start of milestone. Comparing BZY 25 to BZY 75, value of $\sigma_{BZY25}$ was twice than that of BZY 75. Many factors affect to resulted data, but there are no secondary phase and impurity phases. As for the future work, this experiment expands its work scope and applied to thin film electrolyte. In that case, the analysis could show more distinct difference between grain boundaries or other noticeable data.

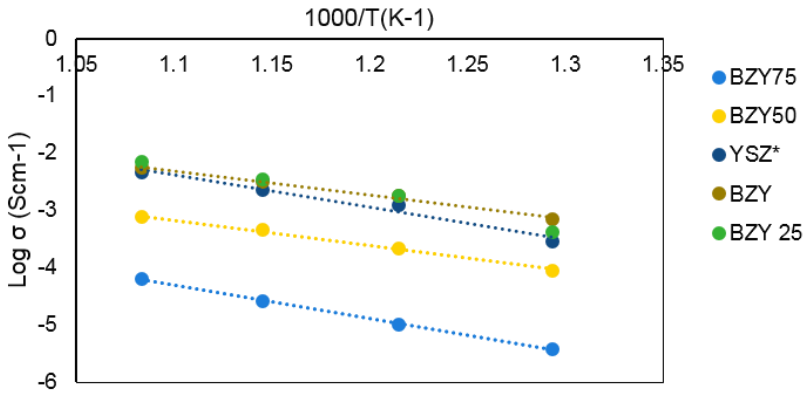


Figure 22. Ionic Conductivity on Air condition

### 3.4.2 Ionic Conductivity on $H_2$ condition

Unlike ambient air condition, wet hydrogen environment result $\sigma_{YSZ} > \sigma_{BZY25} > \sigma_{BZY}$. In thin film studies, BZY conductivity is dominated by proton conduction under a wet hydrogen atmosphere, but in this case interaction with YSZ at grain boundary shows different trends in conductivity plot [23]. As mentioned, YSZ, BZY 25 does not show expected distinct differences, but it could be occurred at the application of thin film. Also, BZY 50 was noticeable for lower activation energy with its slope. Calculated equivalent circuit results that BZY50 has the lowest grain boundary among all. It is a theoretical value to check numerical grain boundary and bulk resistance which means is not an absolute relationship towards its conductivity.

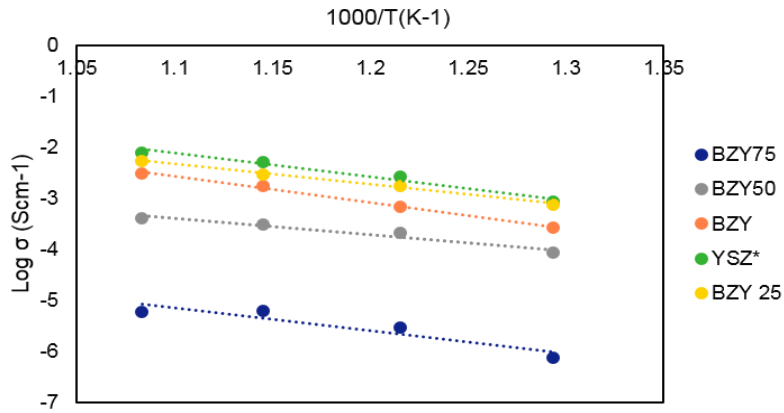


Figure 23. Ionic Conductivity on $H_2$ condition

# Chapter 4. Conclusion

Mixed with protonic conductor material BZY and ionic conductor material YSZ, the hybrid electrolyte BZY-YSZ is aim to work by reversing the drawbacks of the two conducting types of electrolyte. Effect of sintering aid NiO, the microstructure of BZY –YSZ hybrid electrolyte become denser and grain size become smaller than that of raw materials. With smaller grain size, pores from raw materials are clogged and well-percolated to enhance conductivity. The YSZ grains contact on top of BZY grain boundaries. Resulting from the Nyquist plot and Arrhenius plot, BZY 25 shows good performance against all the other samples. However, activation energy of BZY 50 in wet hydrogen environment is noticeable for future work. Applying to Ceria based material and to thin film fuel cell, we expect to see distinct difference between hybrid and raw material in conductivity plot. Therefore, applying hybrid electrolyte to thin film SOFC results promising performance out of primary electrolyte data

# Bibliography


[1] O'Hayre, R., Cha, S.W., Colella W. G.& Prinz, F. B. *Fuel Cell Fundamentals, 3rd ed.* John Wiley & Sons, Hoboken, New Jersey (2016)

[2] Minh, N.Q. *Science, Technology of Ceramic Fuel Cells*, *1st ed*. Elsevier, Amsterdam (1995)

[3] Goodenough, J.B. Oxide-Ion Electrolytes. *Annu. Rev. Mater. Res.* **33**,91-128 (2003).

[4] Shannon, R.D. Revised effective ionic radii and systematic studies of interatomic distances inhalides and chalcogenides, *Acta Crystallogr.* **A 32**, 751(1976).

[5] Serra, J., Meulenberg, W. Thin-Film Proton $BaZr_{0.85}Y_{0.15}O_3$ Conducting Electrolytes: Toward and Intermediate-Temperature Solid Oxide Fuel Cell Alternative. *Journal of American Ceramic Society* **90**, 2082-2089 (2007).

[6] Fabbri, E., Bi, L., Pergolesi, D., Traversa, E. Towards the Next Generation of Solid Oxide Fuel Cells Operating Below 600C with Chemically Stable Proton-Conducting Electrolytes. *Advanced Materials* **24**, 195-208 (2012).

[7] Shafi. S., Bi, L., Boulfrad, S., Traversa., E. Y and Ni Co-Doped $BaZrO_3$ as a Proton-Conducting Solid Oxide Fuel Cell Electrolyte

Exhibiting Superior Power Performance. *Journal of the Electrochemical Society* **162,** F1498-F1503 (2015).

[8] E. Fabbri, D. Pergolesi, and E. Traversa, Materials challenges toward proton-conducting oxide fuel cells: a critical review. *Chem. Soc. Rev*., **39**, 4355 (2010).

[9] H. Iwahara, T. Esaka, H. Uchida, and N. Maeda, Proton conduction in sintered oxides and its application to steam electrolysis for hydrogen production. *Solid State Ionics*, **3-4**, 359 (1981).

[10] E. Fabbri, A. Magras´o, and D. Pergolesi, *MRS Bull*., **39**, 792 (2014).

[11] P. A. Stuart, T. Unno, J. A. Kilner, and S. J. Skinner. Solid oxide proton conducting steam electrolysers. *Solid State Ionics*, **179**, 1120 (2008).

[12] Souza, R., Munir, Z., Kim, S., Martin, M. Defect chemistry of grain boundaries in proton conducting solid oxides. *Solid State Ionics*, **196**, 1-8 (2011).

[13] L. Bi, E. Fabbri, Z. Q. Sun, and E. Traversa. Electrode tailoring improves the intermediate temperature performance of solid oxide fuel cells based on a Y and Pr co-doped barium zirconate proton conducting electrolyte. *Energy Environ. Sci*., **4**, 409 (2011).

[14] L. Bi, E. Fabbri, Z. Q. Sun, and E. Traversa. A novel ionic diffusion strategy to fabricate high-performance anode-supported

solid oxide fuel cells (SOFCs) with proton-conducting Y-doped $BaZrO_3$ films. *Energy Environ. Sci*., **4**, 1352 (2011).

[15] L. Chevallier, M. Zunic, V. Esposito, E. Di Bartolomeo, and E. Traversa. A wet-chemical route for the preparation of Ni–$BaCe_{0.9}Y_{0.1}O_{3-\delta}$ cermet anodes for IT-SOFCs. *Solid State Ionics*, **180**, 715 (2009).

[16] M. Zunic, L. Chevallier, A. Radojkovic, G. Brankovic, Z. Brankovic, E. Di Bartolomeo. Influence of the indium concentration on microstructural and electrical properties of proton conducting NiO–$BaCe_{0.9x}InxY_{0.1}O_{3d}$ cermet anodes for IT-SOFC application. *J. Alloys Compd*., **509**, 1157 (2011).

[16] Park, J. S., Kim, Y.B., Shim, J.H., Kang, S., Gur, T., Prinz, F. Evidence of Proton Transport in Atomic Layer Deposited Yttria-Stabilized Zirconia Films. *Chem. Mater*. **22**, 5366–5370 (2010).

[17] Hui, R., Roller, J., Yick, S., Zhang, X., Deces-Petit, C., Xie, Y., Maric, R., Ghosh, D. A brief review of the ionic conductivity enhancement for selected oxide electrolytes. *Journal of Power Sources*. **172,** 493-502 (2007).

[18] H.L. Tuller, in: O.T. Sorensen (Ed.), *Nonstiochiometric Oxides*, Academic Press, New York, 1981.

[19] R.W. Vest, J.M. Honing, in: N.M. Tallan (Ed.), *Electrical Conductivity in Ceramics and Glass*, Marcel Dekker, New York ,1974.

[20] H. Inaba, H. Tagawa. Ceria-based solid electrolytes. *Solid State Ionics*, **83**, 1 (1996).

[21] B. Zhu. *Solid State Ionics*,**119,** 1-4 (1999).

[22] Jadhav, S.T., Puri, V.R., Jadhav, L.D. NiO-GDC-BCY composites as an anode for SOFC. *Journal of Alloys and Compounds*,**685,**626-632 (2016).

[23] Wang, Z., Liu, M., Li, X., Blinn, K., Lai, S., Lu, Z., Liu, M. Understanding the phase formation and compositions of barium carbonate modified NiO-yittria stabilized zirconia for fuel cell applications. *International Journal of Hydrogen Energy*, **40**, 15597-15604 (2015).

[24] K.-Y. Park, T.-H. Lee, S.Jo, J.Yang, S.-J. Song, H.-T. Lim, J. H.Kim, J.-Y.Park, *J. Power Sources*, **336**, 437 (2016).

[25] Amiri, T., Singh, K., Sandhu, N. J., Hanifi, A. R., Etsell, T. H., Luo, J. L., Thangadurai, V., Sarkar, P. High Performance Tubular Solid Oxide Fuel Cell Based on $Ba_{0.5}Sr_{0.5}Ce_{0.6}Zr_{0.2}Gd_{0.1}Y_{0.1}O_{3-\delta}$ Proton Conducting Electrolyte. *Journal of Electrochemical Society*, **165,** F764-F769 (2018).

[26] Joh, D. W., Park, J. H., Kim, D. Y., Yun, B., Lee, K.T. High performance zirconia-bismush oxide nanocomposite electrolytes for lower temperature solid oxide fuel cells. *Journal of Power Sources*, **320**, 267-273(2016).

[27] Kimpton, T.H., Randle, J., Drennan, J. Conductivity/microstructure study of pyrochlore-type ordered phase in the compound Zr Ce Nd O. *Solid State of Ionics,***154,** 473-480 (2002)

[28] Tschope, A., Birringer, R. Grain size dependence of electrical conductivity in polycrystalline cerium oxide. *J.Electroceram,* **7,**169 (2001).

[29] Diakite, I., Edwards, D., Emerick, B., Raymond, C., Zumbrum, M. Improving a fuel Cell Assembly Process. *MICS Journal*, **6**,22-47 (2014).

# 국문 초록

본 연구에서는 연료전지의 전해질을 이종전해질로 제조함과 동시에 저온에서 작동하는 고체산화물 연료전지용 전해질로 사용 할 수 있는가에 대한 가능성을 연구하고있다.

고체산화물 연료전지는 구조적으로 연료극, 전해질, 공기극으로 구성이 되는데, 공기극의 산소가 산소 이온으로 변환을 하면서 전해질을 통해 확산 이동을 한다. 전해질은 두가지 종류로 나뉘게 되는데, 기존 연구에 주로 사용되는 산소 이온이 확산 이동하는 전해질은 산소 이온 전도성이 높을수록 유리하며 공기 가스 또는 연료 가스가 투과되지 않도록 높은 소결밀도를 확보하는 것이 중요하다. 산소 이온 전해질로 널리 쓰이는 물질은 YSZ (Yttria Stabilized Zirconia)로, YSZ 는 높은 산소 이온 전도성을 가진 물질로서 SOFC 의 전해질로 안정적으로 사용되기에 적합한 특성을 가지고 있지만, 1000℃ 이상의 고온에서 작동해야 하는 문제점이

있다. 다른 한 종류는 수소 이온 전도체 물질로 만든 전해질인데, 수소 이온 전도체 세라믹 중 전도도가 가장 높은 BZY(Barium Yttrium Zirconia) 를 사용하는데 상대적으로 낮은 온도에서 높은 수소이온 전도성을 갖고 있지만 갖을 수 있지만 다공성 구조에 밀도가 높은 전해질을 얻기가 힘든 문제점이 있다.

본 연구에서 말하는 이종전해질이란, 산소 이온 전도체인 (Y2O3)8 (ZrO2)92 와 수소 이온 전도체인 BaZr0.8Y0.2O3 를 각각 25:75, 50:50, 75:25,100:0, 0:100 의 비율로 혼합 하여 BZY 의 다공성 부분을 YSZ 입자로 치밀도를 높힌 전해질을 말한다. 혼합한 파우더를 600°C, 1000°C, 1400 °C 에서 소결을 한 후 밀도가 높아짐을 SEM 으로 확인을 할 수 있었고, 밀도가 높아짐에 따라 BZY, YSZ 만으로 이루어진 전해질 대비 이종 전해질 중 BZY 25: YSZ 75 가 뛰어난 전도도를 보인 것을 확인 할 수 있었다. 전도도의 양극은 Ag paste 을 균일하게 도포한 symmetric cell 의 형태로 기존

공기극 연료극에 수소 연료를 주입하지 않은 공기 중의 상태와 고체산화물 연료전지의 실험 조건과 흡사한 50sccm 의 수소를 연료극에 주입하는 조건에서 측정되었다. 첫번째 조건은 500°C 의 측정온도에서만 BZY25 의 전도도가 BZY 보다 낮고, 550°C 에서 650°C 에서는 BZY 25 의 샘플의 전도도가 가장 높게 측정되었다. 50sccm 의 수소 환경에서는 YSZ 의 전도도와 흡사한 값으로 BZY25 의 전도도가 높게 측정되었다.

본 연구는 bulk 한 구조에서 진행된 것으로 박막에서 요구하는 전도도와는 차이가 있으나, 세리아계 물질을 섞으며 박막에 적용하는 추후 연구를 진행한다면 전기화학적 성능으로도 의미있는 결과가 나올 것으로 사료된다.

**주요어 :** 고체산화물 연료전지, 연료전지, 수소이온 전해질, 프로톤 세라믹 연료전지

**학번 :** 2017-20242